Electronic Supplementary Material (ESI) for ChemComm.

Supplementary Materials for

Gas Phase Identification of the Elusive Oxaziridine (cyclo-H_2CONH) – An Optically Active Molecule

Santosh K. Singh[1], Jesse La Jeunesse[1], Cheng Zhu[1], N. Fabian Kleimeier[1], Kuo-Hsin Chen[2], Bing-Jian Sun[2], Agnes H. H. Chang[2*], Ralf I. Kaiser[2*]

[1]*Department of Chemistry, University of Hawaii, 2545 McCarthy Mall, 96822 HI, USA.*
W. M. Keck Research Laboratory in Astrochemistry, University of Hawaii, 96822 HI, USA.

[2]*Department of Chemistry, National Dong Hwa University, Shoufeng, Hualien 974, Taiwan.*

Correspondence to: ralfk@hawaii.edu, hhchang@gms.ndhu.edu.tw

This PDF file includes:

Materials and Methods

Experimental

Experiments were conducted in an ultrahigh vacuum chamber evacuated to a base pressure of a few 10^{-11} torr using turbo molecular pumps backed by dry scroll pumps.[1, 2] To prepare each ice mixture, gases of methane (CH_4; 99.95% Sigma Aldrich) and nitrogen monoxide (NO; 99.95% Sigma Aldrich) were premixed and deposited at 5×10^{-8} torr via glass capillary onto a silver substrate which is mounted on a cold finger made from oxygen free high conductivity copper. The temperature of the cold finger was maintained at 4.9 ± 0.2 K using closed cycle helium refrigerator (Sumitomo Heavy Industries, RDK-415E) during deposition of the gases. The ice mixtures of ^{13}C-methane ($^{13}CH_4$) and nitrogen monoxide (NO) as well as deuterated-methane (CD_4) and NO were prepared in the similar way. The thickness of each ice of 743 ± 50 nm was determined in situ via laser interferometry (for details see Figure S5). The infrared spectra of the ice mixtures were collected in the 6000-600 cm^{-1} region using a Fourier Transform Infrared Spectrometer (Nicolet 6700) operated at a resolution of 4 cm^{-1}. The ratio of nitrogen monoxide (NO) to methane (CH_4) in the ice mixture was found to be 1.1 ± 0.4 :1, based on the column densities of NO and CH_4 calculated using a modified Lambert-beer law equation.[3] The column densities of nitrogen monoxide (NO; 1.29 ± 0.3 × 1017 molecules cm^{-2}) and methane (CH_4; 1.23 ± 0.2 × 1017 molecules cm^{-2}) were determined using integrated area of the ν_1 band (1860 cm^{-1}) of NO and ν_4 band (1297 cm^{-1}) of CH_4 with their absorption coefficients of 9.2×10^{-18} and 1.40×10^{-17} cm $molecule^{-1}$, respectively.[4, 5] Then, each ice mixture was exposed to 5 keV energetic electrons at an angle of 70º to the normal of the substrate at an electron current of 20 ± 2 nA for 15 min. IR spectra of the ices were measured in situ during irradiation to monitor the changes induced by ionizing radiation. Using Monte Carlo simulations via CASINO 2.42 software,[6] the average penetration depth of the electrons in the ice mixture was found to be 317 ± 30 nm and the average energy deposited was calculated to be 0.44 ± 0.04 eV $molecule^{-1}$ for methane and 0.82 ± 0.08 eV $molecule^{-1}$ for nitrogen monoxide (Table S6). Hereafter, ices were annealed at a rate of 1 K min^{-1}, and molecules subliming from the substrate were ionized and detected using photoionization along with reflectron time-of-flight mass spectrometry (PI-ReTOF-MS). Pulsed VUV light is utilized for the photoionization of the molecules. Five VUV energies at 10.49 eV, 9.95 eV, 9.92 eV, 9.50 and 9.00 eV were used to differentiate between

isomers of oxaziridine (Table S7). The ions formed are extracted and eventually separated based on their mass-to-charge (m/z) ratio before reaching to microchannel plate (MCP) detector. The MCP detector generates a signal when ions reach to the detector. This signal is amplified using a preamplifier (Ortec 9305) and shaped with a 100 MHz discriminator. The discriminator sends the signal to a computer based multichannel scaler, which records the signal in 4 ns bins triggered at 30 Hz by a pulse delay generator. 3600 sweeps were collected for each mass spectrum per 1 K increase in the temperature during the TPD phase.

Computational

The reactions between carbene (CH_2) and nitrosyl hydride (HNO) proceeding on the triplet and singlet potential energy surfaces (PESs) are investigated. Collision complexes were identified, their mutual conversion and subsequent isomerization of cyclo-H_2CONH (1) were characterized. The geometries of these species and transition states were optimized along with the harmonic frequencies by utilizing coupled cluster CCSD/cc-pVTZ calculations. Their CCSD(T)/cc-pVDZ, CCSD(T)/cc-pVTZ, and CCSD(T)/cc-pVQZ energies were computed and extrapolated to complete basis set limits, CCSD(T)/CBS, with CCSD/cc-pVTZ zero-point energy corrections. These energies are expected to be accurate within 4 kJ mol^{-1}.[7] The triplet - singlet minimum energy crossing points (MSX) were located with CPMCSCF[8]/TZVPP method with energy refined via CCSD(T)/CBS. The intrinsic reaction coordinate (IRC) calculations at CCSD/cc-pVTZ//CCSD(T)/CBS level were carried out to probe the entrance of singlet CH_2 + HNO → 1, 2, 7 channels. The GAUSSIAN 16 program[9] was employed in coupled cluster calculations, and MOLPRO[8] was used for the surface-crossing.

Generation of VUV light

1. 10.49 eV –The third harmonics (355 nm) of a pulsed ND:YAG laser (Spectra Physics, PRO-250-30; 30 Hz) is exploited for generating 10.49 eV VUV light. The 355 nm light was focused on pulsed jet of Xenon (80 μs, 30 Hz) which results in generation of 118 nm light (10.49 eV) via non-linear mixing. The 10.49 eV light was separated from 355 nm light by a LiF biconvex lens (ISP Optics) and directed 2 mm above the sample to ionize the subliming molecules.

2. 9.95 eV – The second harmonics (532 nm) of a pulsed ND:YAG laser (Spectra Physics, PRO-250-30; 30 Hz, 10 ns) was used to pump a dye laser (Sirah Cobra Stretch) having Rhodamine 610/640 dye mixture. The fundamental output of the dye laser (606.948 nm) undergoes frequency tripling to generate 202.316 nm (ω1) light. Two photons of ω1 is required to access the resonant transition of Krypton. The third harmonics (355 nm) of a second ND:YAG laser (Spectra Physics, PRO-250-30; 30 Hz, 10 ns) was used to pump another dye laser (Sirah Cobra Stretch) containing Coumarin 540 A dye to generate 537.550 nm (ω2) light. The 202 nm and 537.550 nm lights were spatially and temporally overlapped on pulsed jet of Krypton (80 μs, 30 Hz) which act as a non-linear medium. Difference frequency mixing of two photons of ω1 and one photon of ω2 in Krypton (2ω1-ω2) results in the generation of 124.61 nm (ω_{VUV} = 9.95 eV) light. A LiF biconvex lens is used to separate the 124.61 nm light from residual 202 and 537.550 nm lights.

3. 9.92 eV – The 124.98nm (9.92 eV) light was generated via difference frequency mixing of two photons of 202.316 nm (ω1) and one photon of 532 nm (ω2) light in krypton. The process of producing 202.316 nm light has been discussed in the generation of 9.95 eV light. The 532 nm light is generated by frequency doubling the fundamental output (1064 nm) of a pulsed ND:YAG laser. The 202.316 nm (ω1) and 532 nm (ω2) lights were spatially and temporally overlapped on pulsed jet of Krypton for difference frequency generation of 9.92 eV light, which is eventually separated from the residual ω1 and ω2 through a LiF biconvex lens. The generated 9.92 eV light is directed at about 2 mm above the sample to ionize the subliming molecules.

4. 9.50 eV – Difference frequency mixing of two photons of 202.316 nm (ω1) and one photon of 449.794 nm (ω2) in Krypton results in generation of 130.51 nm (9.70 eV) light. The process of producing 202.316 nm is identical to that of described in the generation of 9.95 eV light. To generate 449.794 nm light, a dye laser containing Coumarin 450 dye was pumped by the third harmonics (355 nm) of a ND:YAG laser. Both ω1 and ω2 were spatially and temporally overlapped on the pulsed jet of Krypton for difference frequency generation of 130.51 nm light. The 130.51 nm light generated is eventually separated from the residual 202.316 nm and 449.794 nm lights by the help of LiF biconvex lens and directed at about 2 mm above the sample to ionize the subliming molecules.

5. 9.00 eV – The 124.98 nm (9.92 eV) light was generated via difference frequency mixing of two photons of 222.566 nm (ω1) and one photon of 579.014 nm (ω2) light in xenon. To produce ω1, the fundamental output of a dye laser (445.132, Coumarin 450), pumped by the third harmonics (355 nm) of an ND:YAG laser (Spectra Physics, PRO-250-30; 30 Hz, 10 ns), was frequency doubled through a BBO crystal. The second harmonics (532 nm) of a pulsed ND:YAG laser was used to pump another dye laser having Pyrromethane 593 dye to generate ω2 (579.014 nm). The ω1 and ω2 lights were spatially and temporally overlapped on the pulsed jet of Krypton for difference frequency generation of 124.98 nm light. The 124.98 nm light generated is eventually separated from the residual 222.566 nm and 579.014 nm lights by the help of a LiF biconvex lens and directed at about 2 mm above the sample to ionize the subliming molecules.

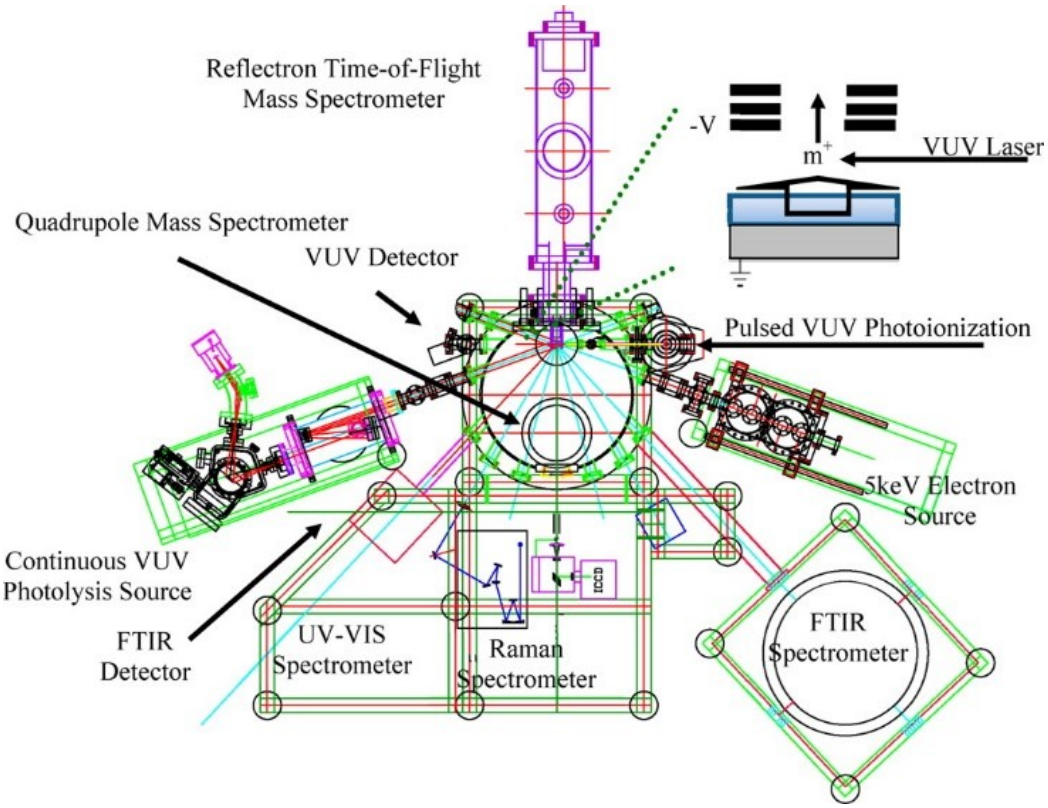

Fig. S1. Schematic top view of the ultra-high vacuum chamber including the electron source, analytical instruments (FTIR, UV-VIS, ReTOF), and cryogenic target (point of convergence lines)[1, 10].

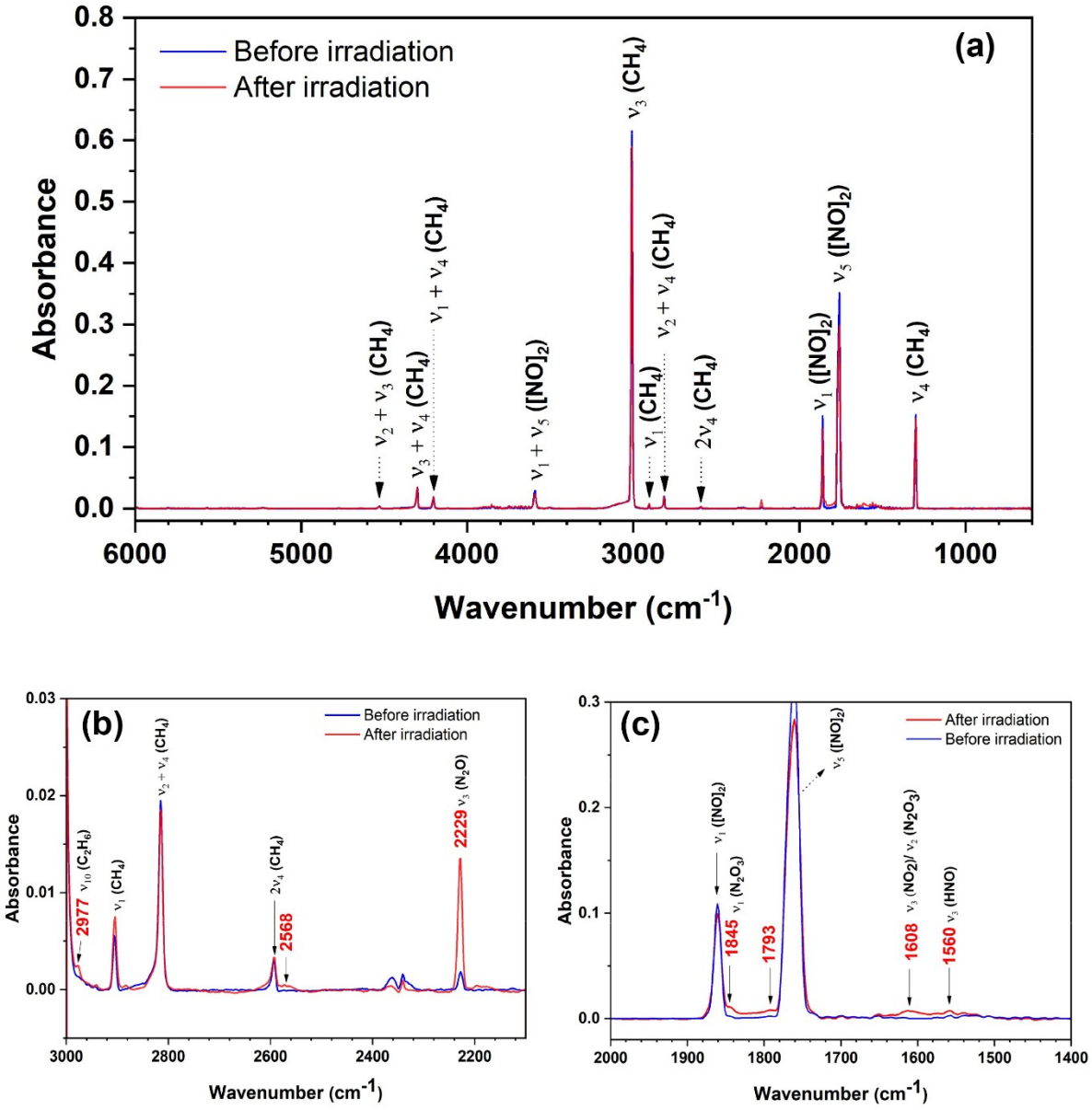

Fig. S2. (a) FTIR spectra of the methane (CH_4) and nitrogen monoxide (NO) ice mixture before and after the irradiation. Spectral regions 3000-2000 and 2000-1400 cm^{-1} are magnified in (b) and (c) respectively for better visibility. Detailed assignments of the bands are provided in Table S2. New bands observed after irradiation are indicated in red color.

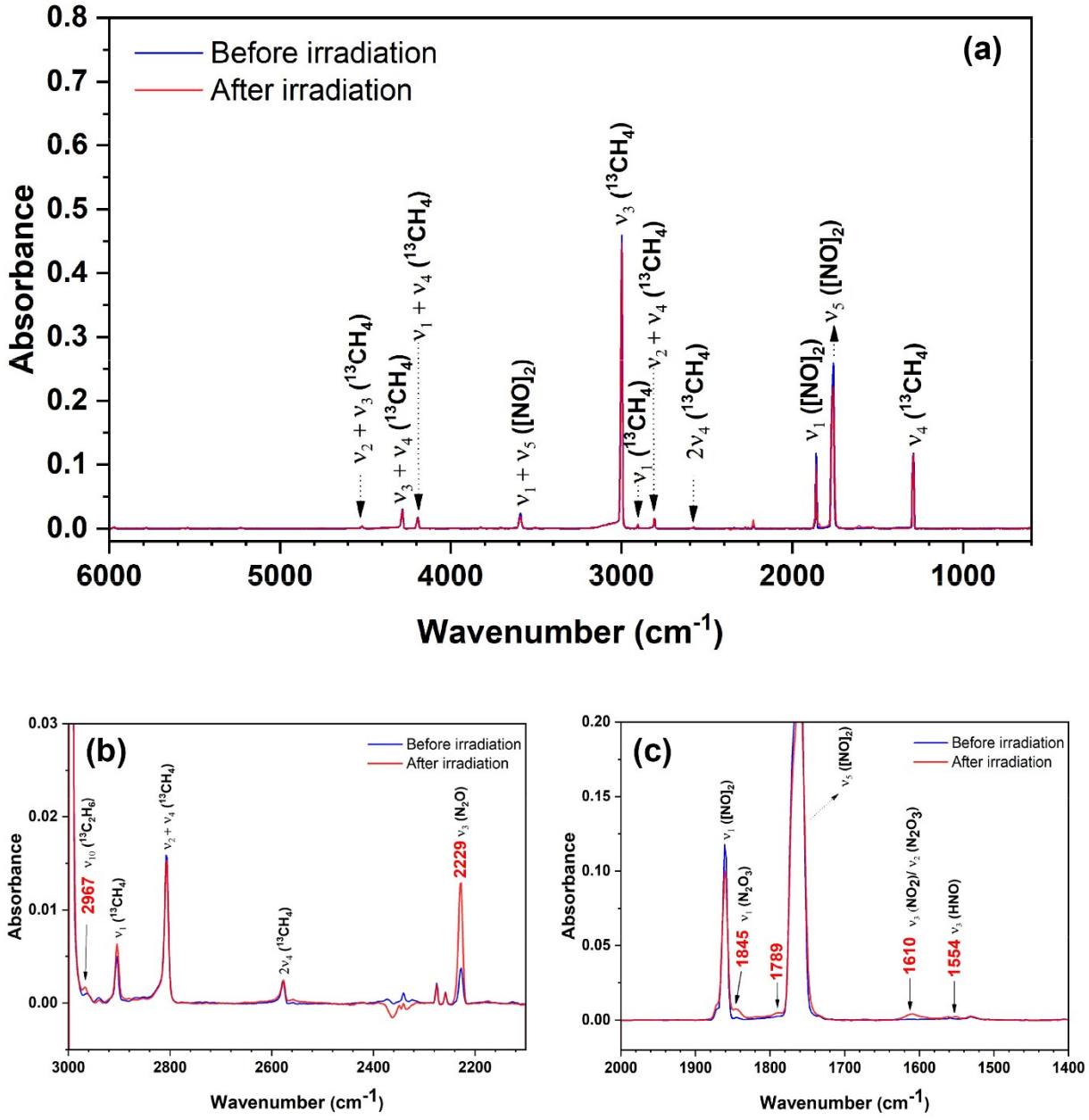

Fig. S3. (a) FTIR spectra of the ^{13}C-methane ($^{13}CH_4$) and nitrogen monoxide (NO) ice mixture before and after the irradiation. Spectral regions 3000-2000 and 2000-1400 cm^{-1} are magnified in (b) and (c) respectively for better visibility. Detailed assignments of the bands are provided in Table S3. New bands observed after irradiation are indicated in red color.

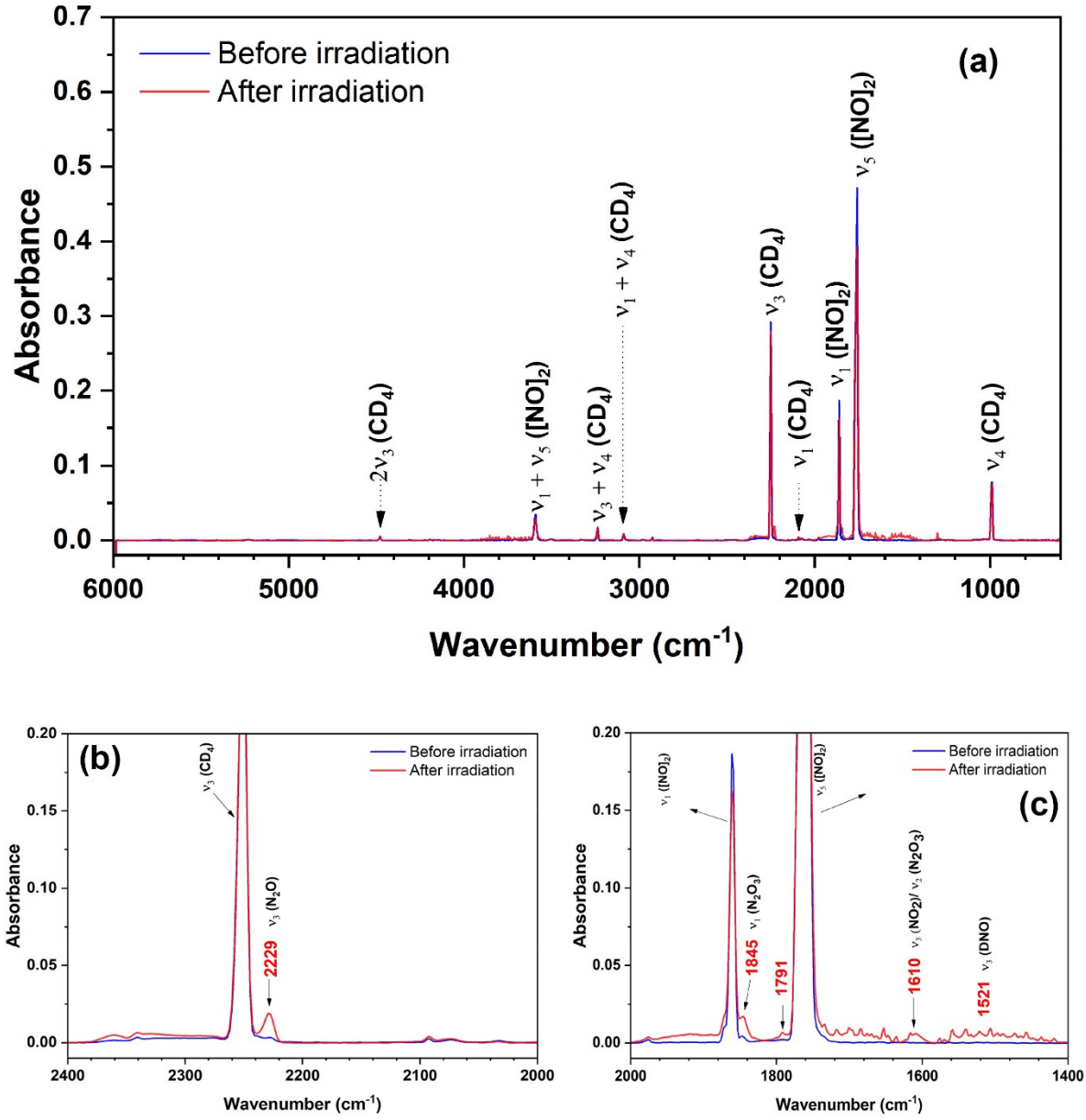

Fig. S4. (a) FTIR spectra of the D4-methane (CD_4) and nitrogen monoxide (NO) ice mixture before and after the irradiation. Spectral regions 2400-2000 and 2000-1400 cm^{-1} are magnified in (b) and (c) respectively for better visibility. Detailed assignments of the bands are provided in Table S4. New bands observed after irradiation are indicated in red color.

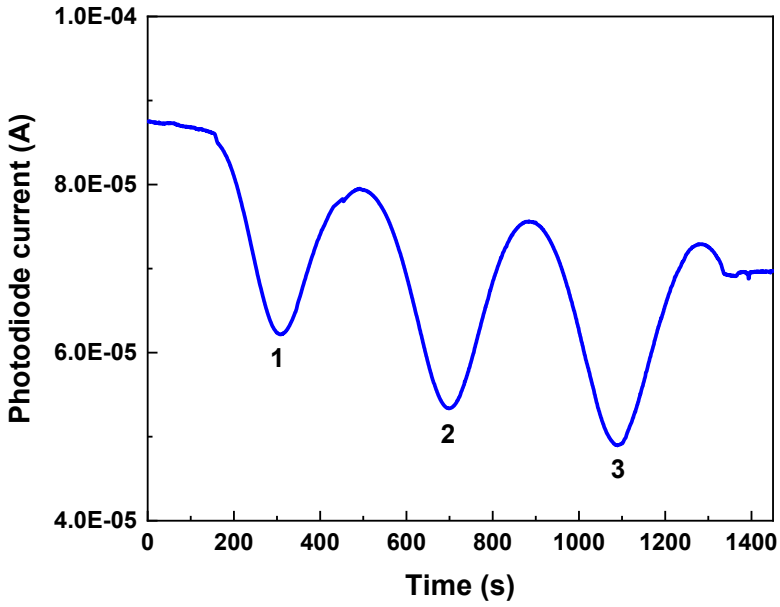

Fig. S5. Interference pattern measured during the deposition of a CH_4 + NO gas mixture for a 632.8 nm laser at an angle of incidence of 4°. Number of fringes are labelled below the signal minima.

The thickness of the ice (d) was determined using laser interferometry. A He-Ne laser of 632.8 nm wavelength (λ) has been used at an angle of incidence (θ) equal to 4° to measure the interference. Three interference fringes (m = 3) was observed during the deposition of the ice as shown in Figure S5.

The average refractive index of the ice mixture (n_{ice} = 1.28) was determined from the refractive indices of the neat nitrogen monoxide (n = 1.25)[4] and methane ices (n = 1.33)[5] reported in the literature. Using the equation given below

$$d = \frac{m\lambda}{2\sqrt{n^2 - \sin^2\theta}} \quad (1)$$

the thickness of the NO + CH_4 ice mixture was determined to be 743 ± 50 nm.

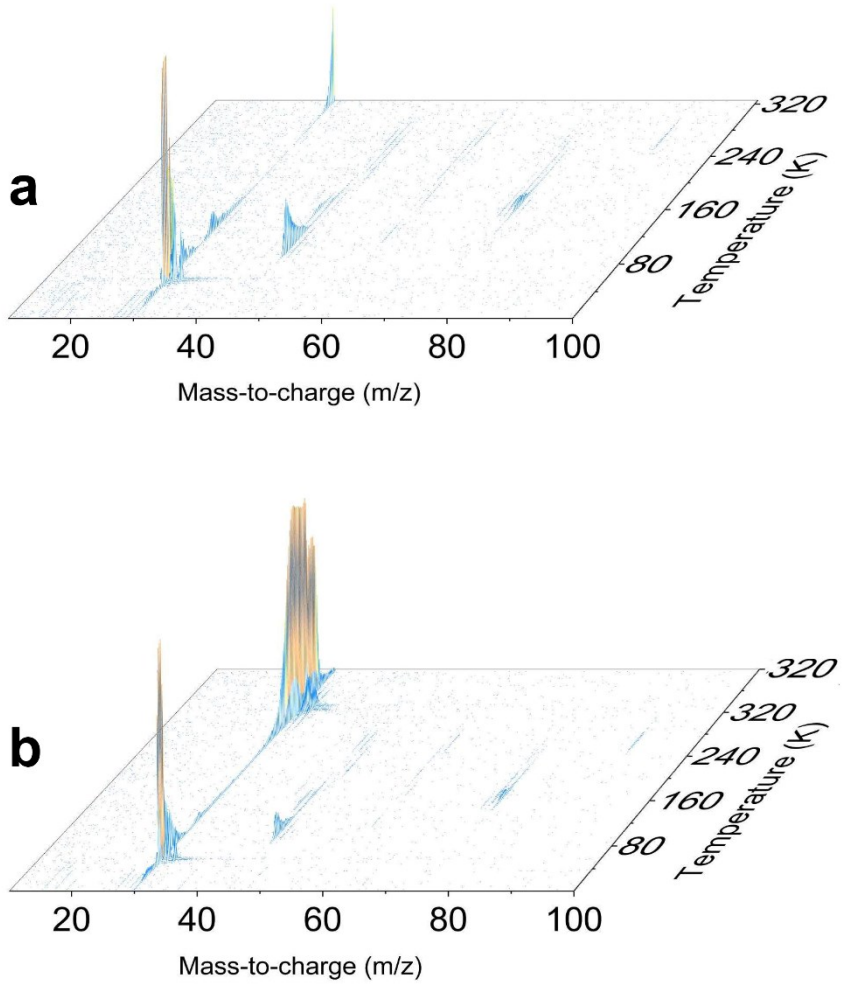

Fig. S6. PI-ReTOF mass spectra measured at photon energies of (a) 9.95 eV and (b) 9.92 eV during the TPD phase of irradiated methane (CH_4) and nitrogen monoxide (NO) ice mixture.

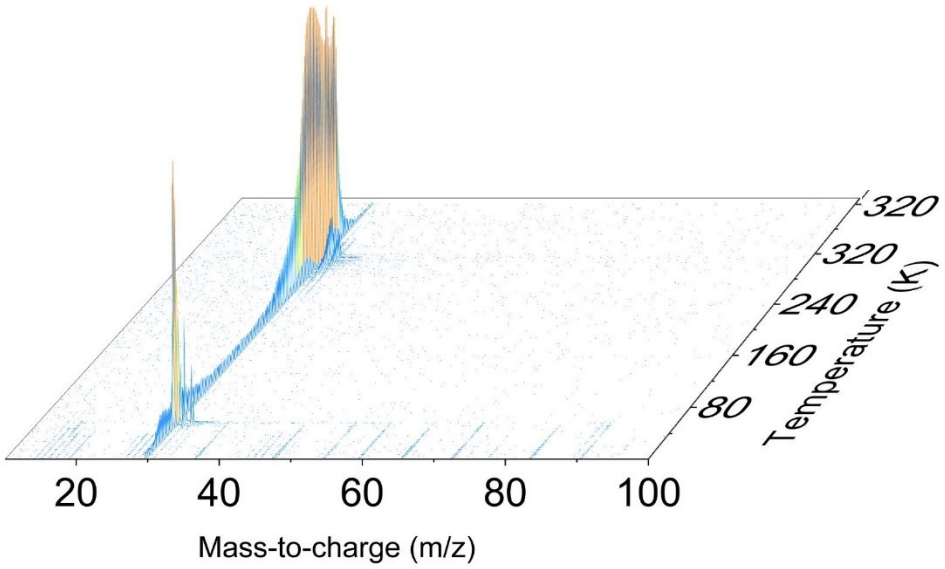

Fig. S7. PI-ReTOF mass spectrum measured at a photon energy of 10.49 eV during the TPD phase of non-irradiated methane (CH_4) and nitrogen monoxide (NO) ice mixture i.e. blank experiment.

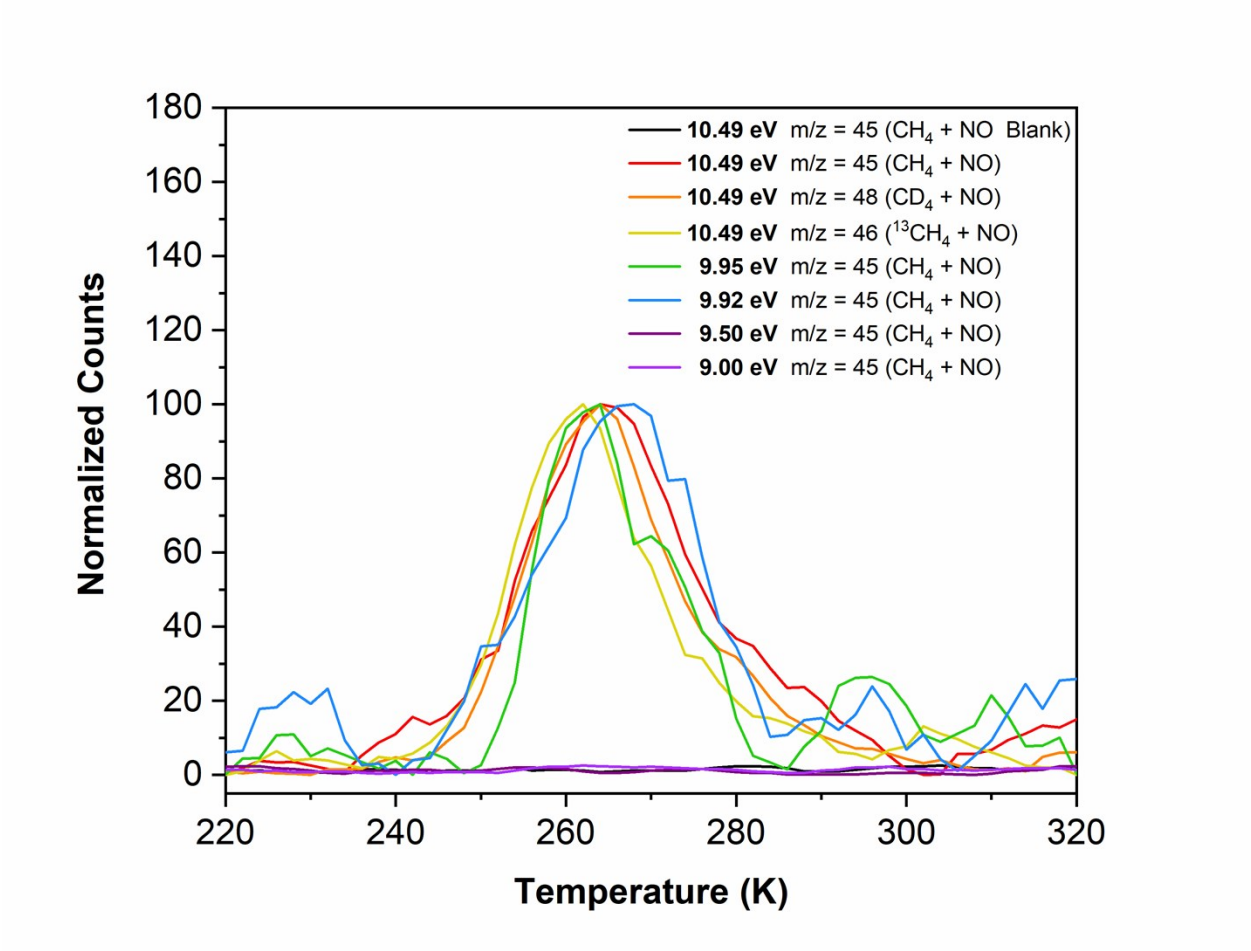

Fig. S8. Normalized temperature program desorption (TPD) profiles measured at mass-to-charge ratio of 45 at photoionization energies of 10.49, 9.95, 9.92, 9.50 and 9.00 eV, during the TPD phase of the irradiated methane (CH_4) and nitrogen monoxide (NO) ice mixtures. For comparison, the TPD profiles measured at m/z = 46 and 48 in the irradiated $^{13}CH_4$ + NO and CD_4 + NO ice mixtures respectively, at a photoionization energy of 10.49 eV are also included.

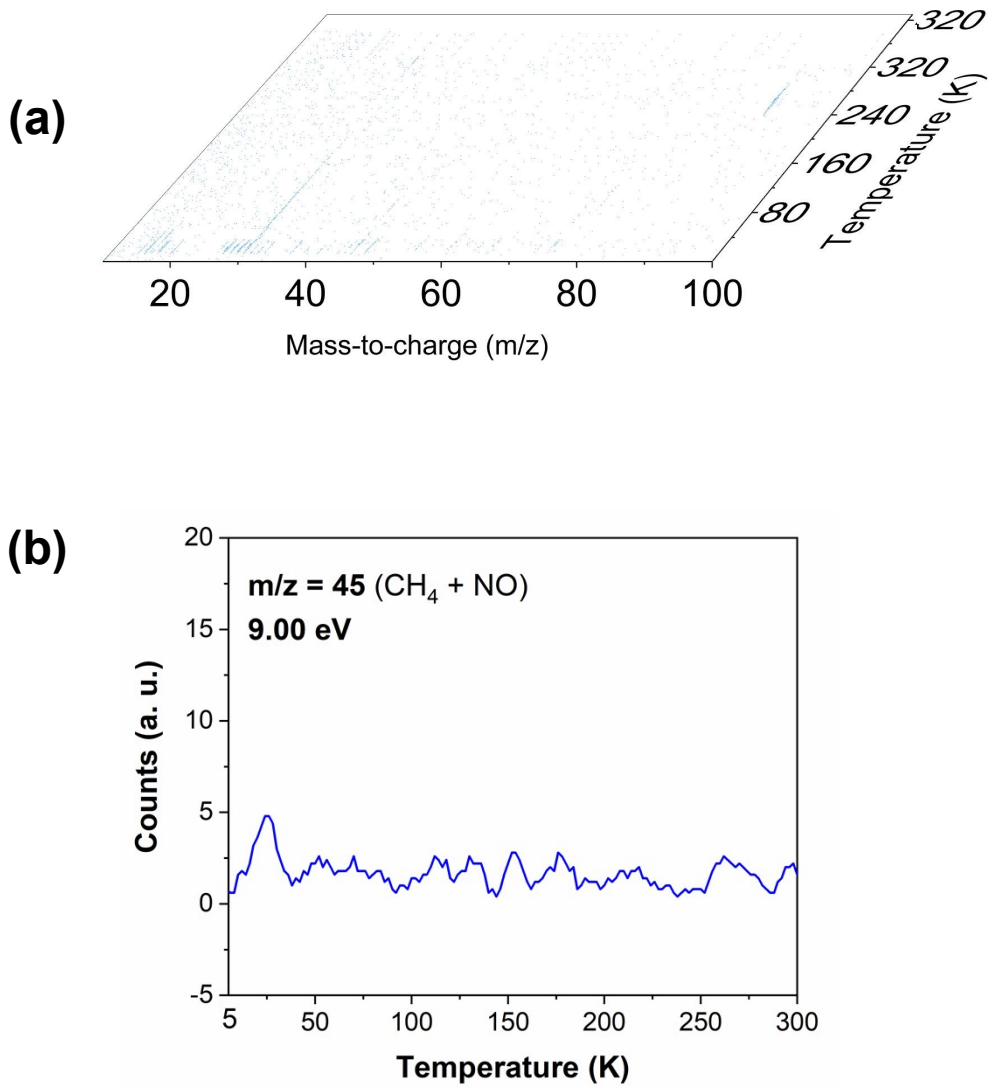

Fig. S9. (a) PI-ReTOF mass spectrum measured at a photoionization energy of 9.00 eV during the temperature program desorption (TPD) phase of the irradiated methane (CH_4) and nitrogen monoxide (NO) ice mixture. (b) TPD profile recorded at mass-to-charge value of 45 in the mass spectrum depicted in figure (a).

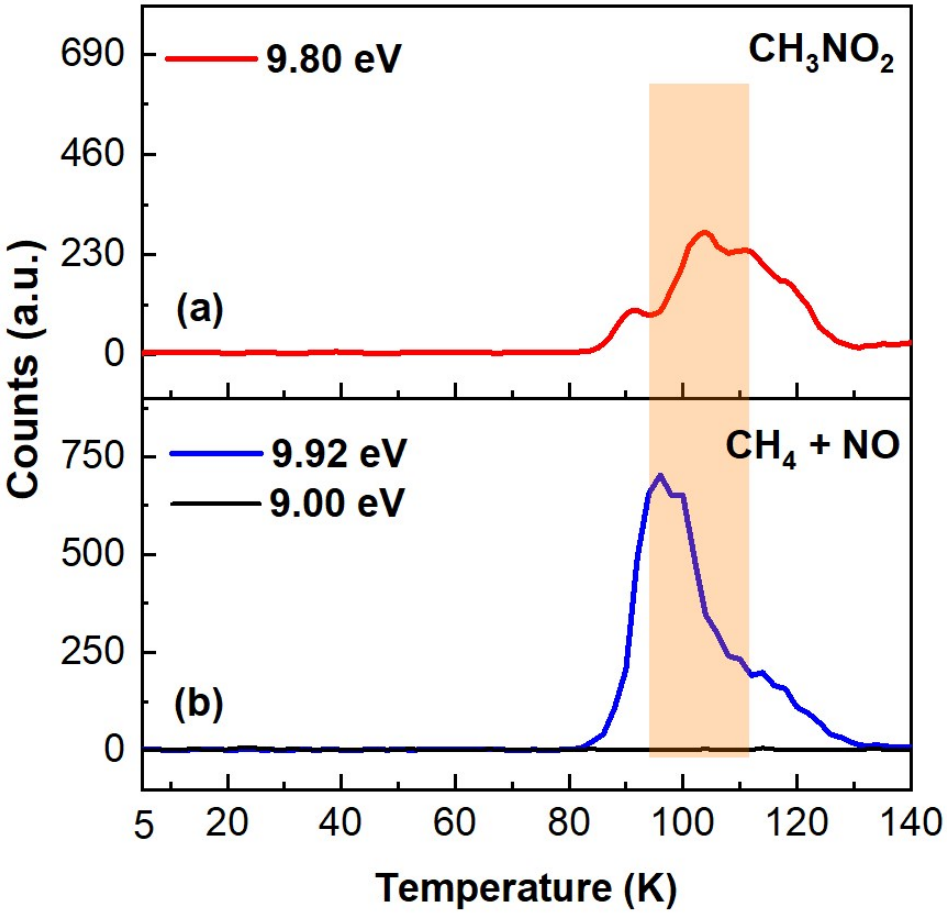

Fig. S10. (a) TPD profile of nitrosomethane measured at m/z = 45 in nitromethane (CH_3NO_2) matrix exploiting PI-ReTOF mass spectrometer at photon energy of 9.80 eV. Nitrosomethane was generated in-situ via decomposition of nitromethane. (b) TPD profile measured at m/z = 45 at photon energies of 9.92 and 9.00 eV after irradiation of CH_4 + NO binary mixture.

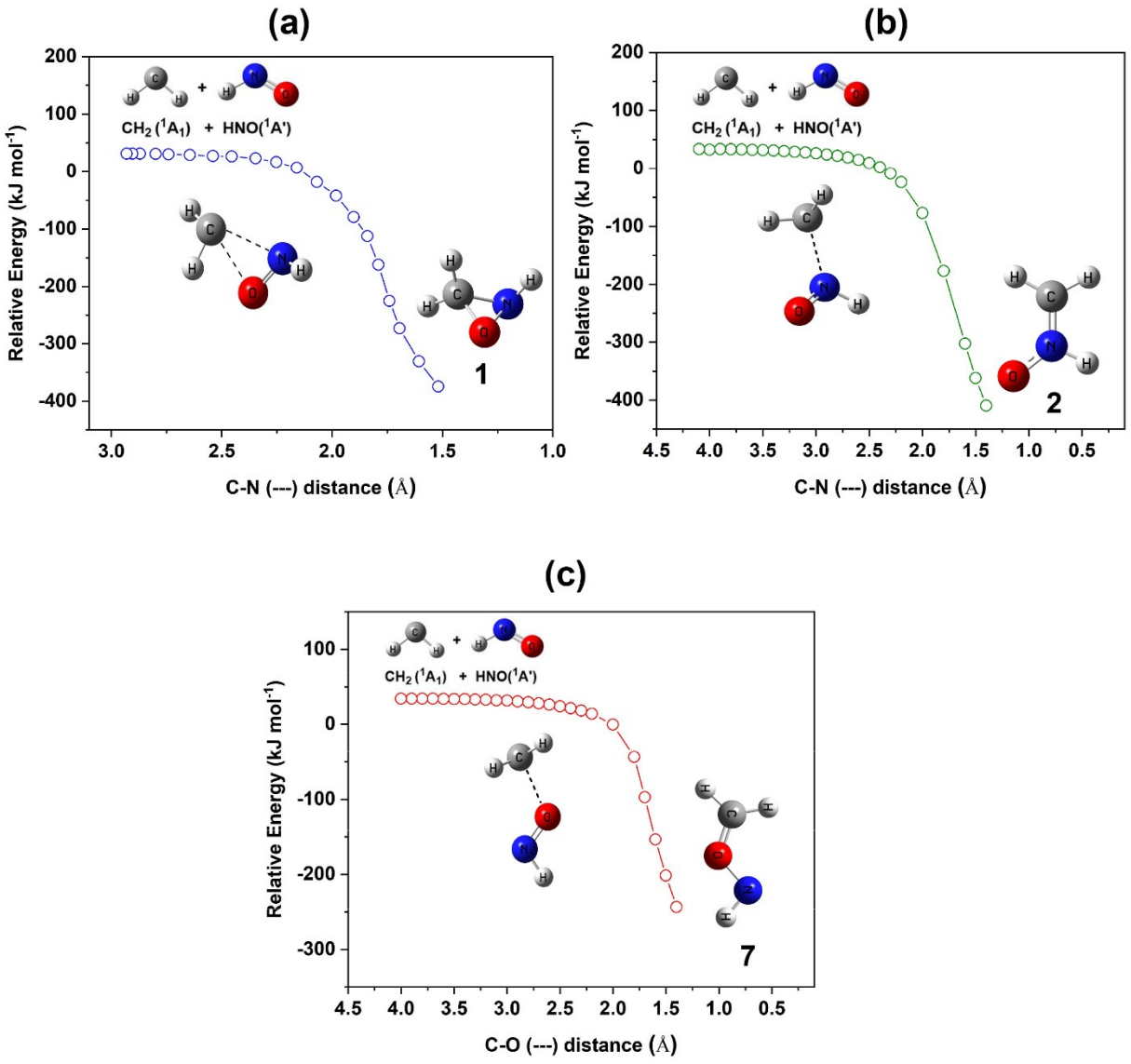

Fig. S11. Intrinsic reaction coordinate (IRC) calculations at the CCSD/cc-pVTZ//CCSD (T)/CBS level of theory, for the formation of CH_3NO isomers (a) **1**, (b) **2,** and (c) **7** via addition of singlet carbene (CH_2) to N=O bond, nitrogen atom and oxygen atom of the nitrosyl hydride (HNO) respectively.

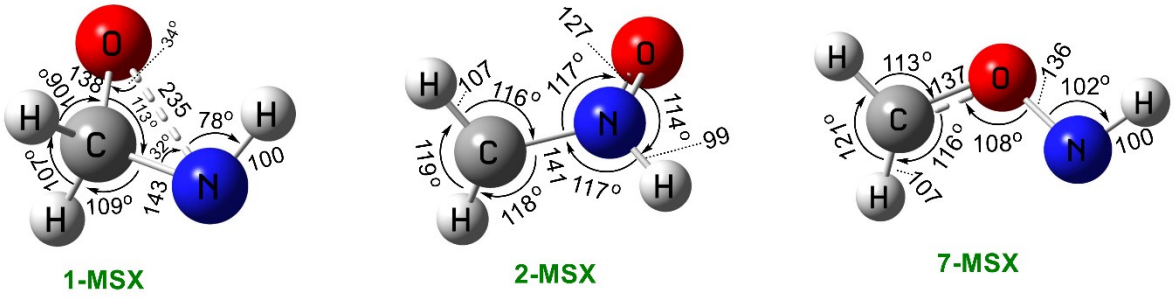

Fig. S12. The CPMCSCF/TZVPP//CCSD(T)/CBS calculated structures of minimum-energy crossing points (MSX) corresponding to Figure 4.

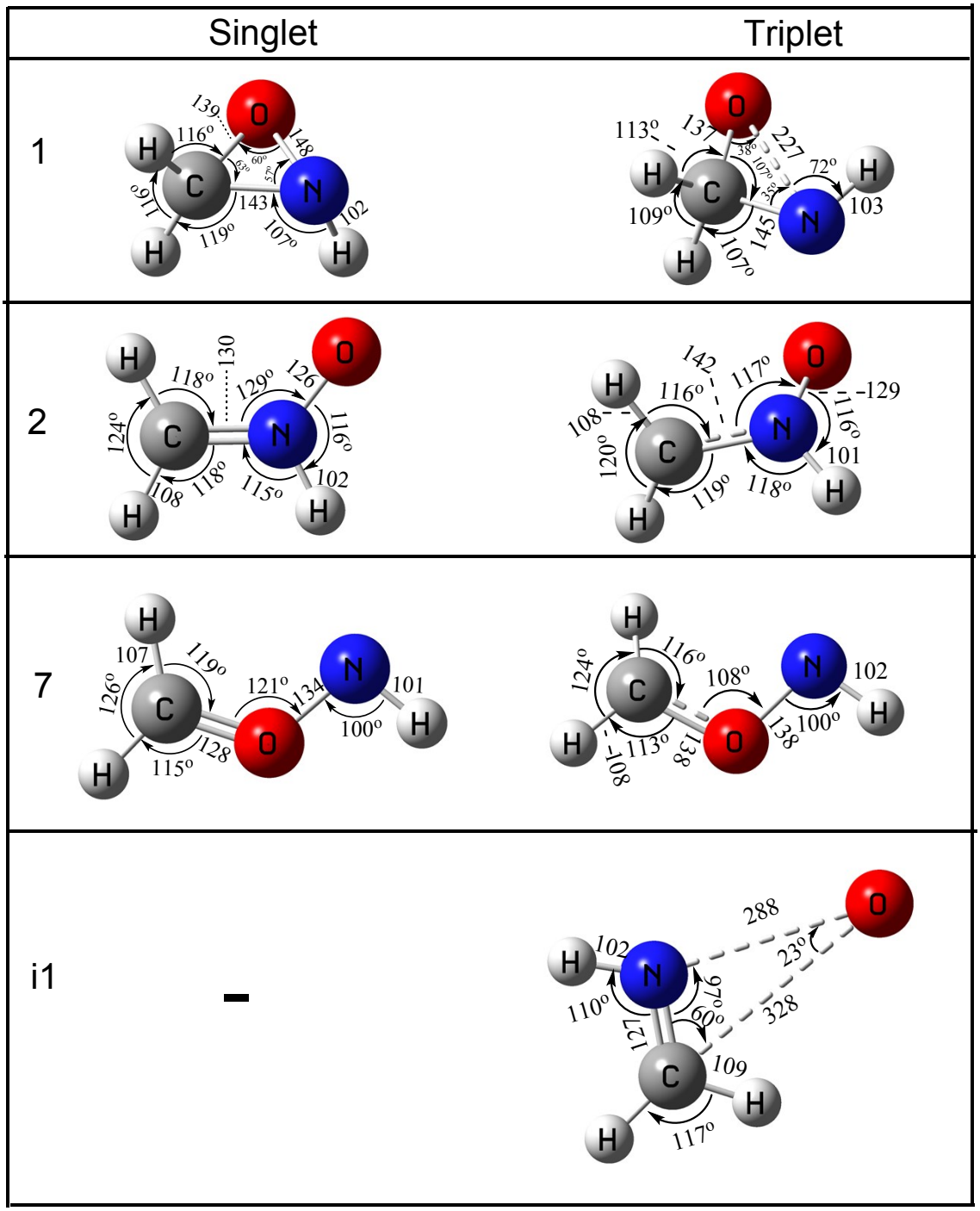

Fig. S13. Geometrical parameters of singlet and triplet structures of CH_3NO isomers (1, 2 and 7) as well as triplet intermediate complex i1. Bond lengths are in pm and bond angles are in degrees.

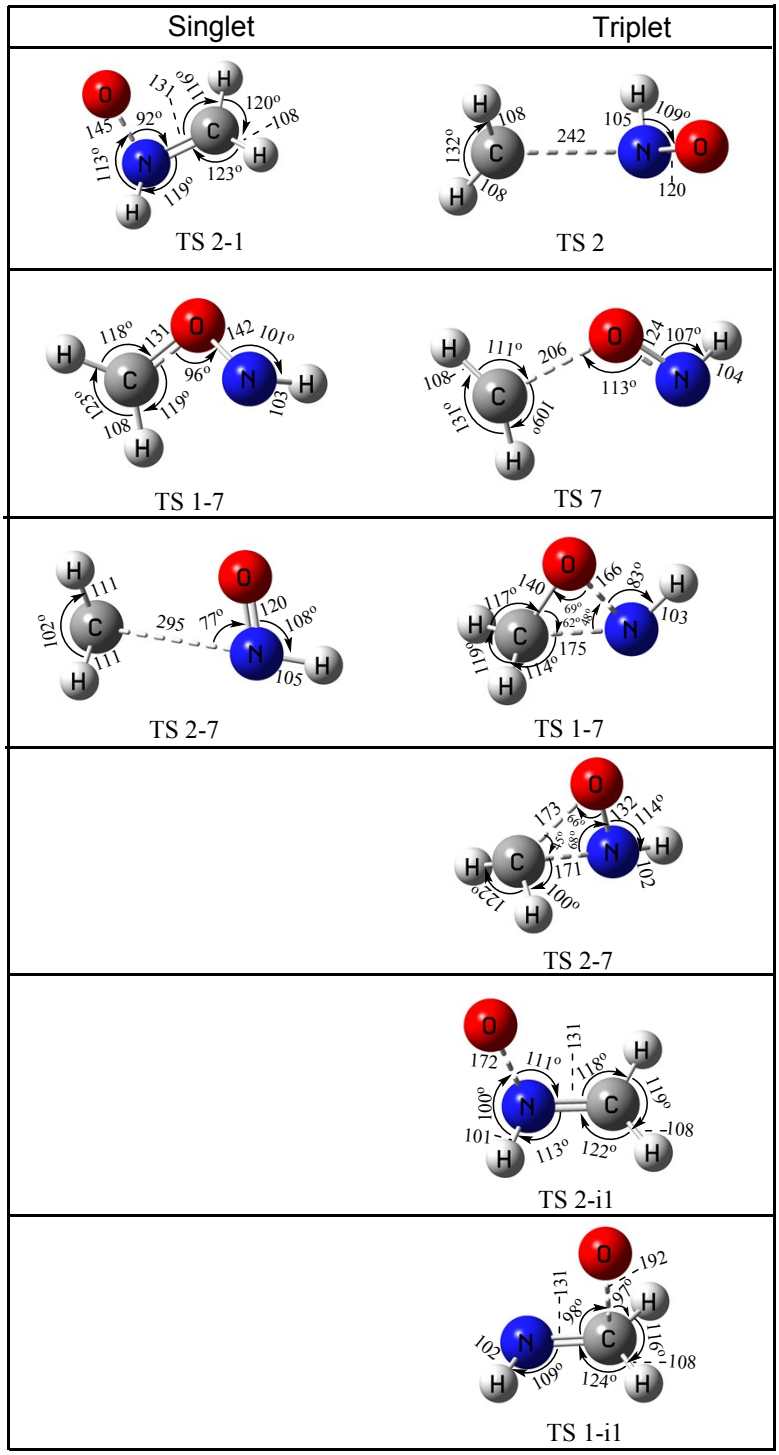

Fig. S14. Structures and geometrical parameters of the transition states in the reactions of singlet and triplet carbene with nitrosyl hydride (HNO) depicted in Figure 4. Bond lengths are in pm and bond angles are in degrees.

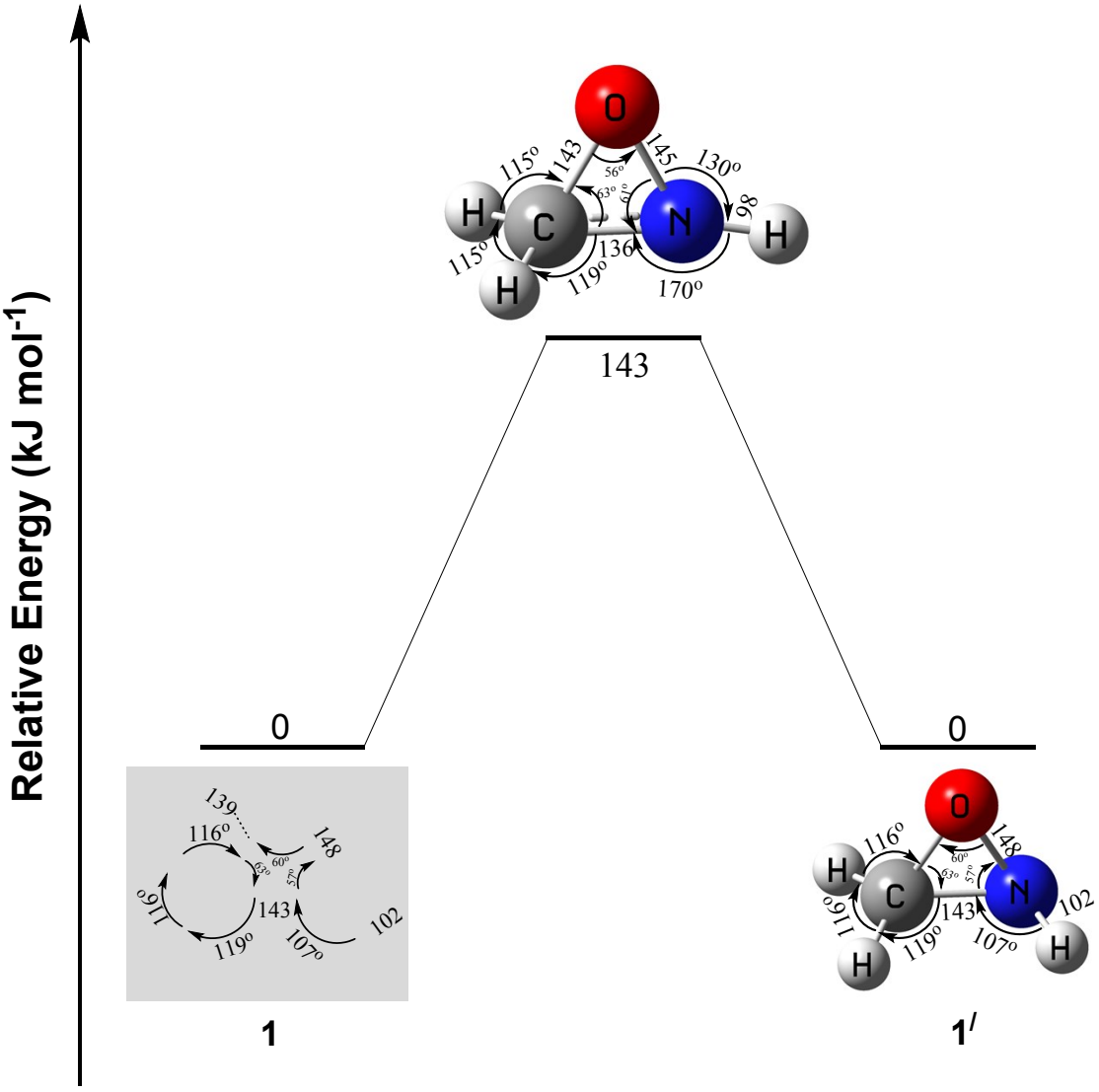

Fig. S15. Computed (CCSD/cc-pVTZ//CCSD(T)/CBS level) ring inversion barrier of isomer 1 on the adiabatic singlet potential energy surface.

Table S1. Calculated adiabatic ionization energies (IE) and the relative energies (E_{rel}) of distinct CH_3NO isomers.

						Error limits		
	Name / Formula	**Structure**	**E_{rel} (kJ mol^{-1})**	**IE (eV) Comp.**	**IE (eV) Exp.**	**IE (Comp.-Exp.) Upper limit**	**IE (Comp.-Exp) Lower limit**	**IE range***
1	N-H Oxaziridine H_2CONH	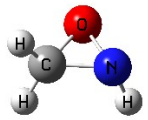	297	9.80	–	-	-	9.83-9.75
2	N-oxide Methanimine H_2CNHO	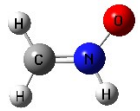	260	9.44	–	-	-	9.47-9.42
3	Nitrosomethane CH_3NO	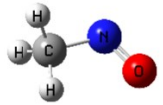	262	9.25	9.3†	-0.05	-	9.28-9.20
4	Formaldehyde oxime H_2CNOH	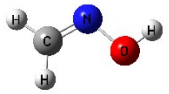	211	10.04	10.1†	-0.06	-	10.08-9.99
5	Methanimidic Acid NHCHOH	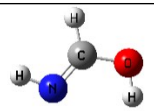	47	10.25	–	-	-	10.28-10.20
6	Formamide NH_2CHO	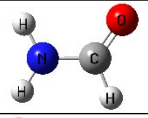	0	10.25	10.25 ± 0.02†	-0.02	+0.02	10.28-10.20
7	(Methyleneoxonio) amide $H_2CO(NH)$	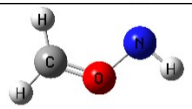	424	8.57	-	-	-	8.60-8.56
						Average -0.04 ± 0.02	Average +0.02	
						Combined error limits -0.06 to +0.02		

†Values from NIST database. * IE range is determined by including the error limits in the calculated IE and subtracting 0.03 eV to include the stark effect.

Table S2. Experimental and computed adiabatic ionization energies of various molecules.

Name	Structure	Ionization energy (eV)		Error
		Calculated	Experimental	
N-methyl formamide	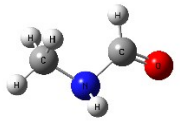	**9.80**[1]	**9.83**[a]	-0.03
Acetamide	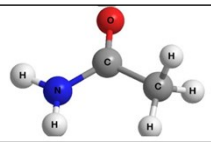	**9.74**[1]	**9.69** [a]	-0.05
Methylenimine	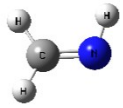	**9.94**[2]	**9.88** [b]	-0.06
1,1-Dimethylhydrazine	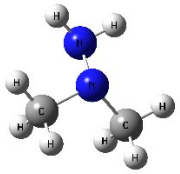	**7.24**[2]	**7.29** [c]	-0.05
Trans-methyl nitrite	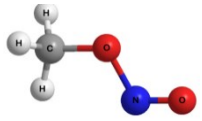	**10.31**[3]	**10.38** [d]	+0.07
Trans-nitrosomethane dimer	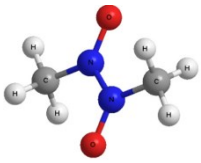	**8.38**[3]	**8.3**[e]	-0.08

[a] National Institute of Standards and technology (NIST) U.S. Department of Commerce, [b]Tarasenko, N.A.; et al. *Adiabatic ionization energy of methylenimine*, **Bull. Acad. Sci. USSR, Div. Chem. Sci.** 1986, 10, 2196. [c]Mautner(Meot-Ner), M. et al. *Special effects of an unusually large neutral to radical cation geometry change. Adiabatic ionization energies and proton affinities of alkylhydrazines*, **J. Am. Chem. Soc.**, 1984, 106, 7384. [d]Gilman, J.P. et al. *Competition between isomerization and fragmentation of gaseous ions. II. Nitromethane and methylnitrite ions*, **J. Chem. Phys.**, 1983, 78, 1174. [e]Frost, D.C. et al. *A study by He I photoelectron spectroscopy of monomeric nitrosomethane, the cis and trans dimers, and formaldoxime*, **J. Phys. Chem.**, 1982, 86, 3577. [1]Calculated values reproduced from reference R. Frigge et al. ApJ. 2018, 862, 84. [2]Calculaed values reproduced from reference C. Zhu et al. Phys.Chem.Chem.Phys., 2019, 21, 1952. [3]Calculaed values reproduced from reference P. Maksyutenko et al. Chem. Phys. Lett., 2016, 658, 20–29.

Table S3. Infrared absorption features of CH_4 and NO ice mixture before irradiation and new absorption bands observed in the infrared spectrum after irradiation. All measurements have been performed at 5K.

Wavenumber (cm^{-1})		Assignment	Carrier	Ref.
Before irradiation	**After irradiation**			
4530		$\nu_2 + \nu_3$ (CH_4)	combination	5
4300		$\nu_3 + \nu_4$ (CH_4)	combination	5
4202		$\nu_1 + \nu_4$ (CH_4)	combination	5
3592		$\nu_1 + \nu_5$ ($[NO]_2$)	combination	4
3008		ν_3 (CH_4)	CH stretch	5
	2977	ν_{10} (C_2H_6)	CH_3 stretch	5
2904		ν_1 (CH_4)	Symm. stretch	5
2813		$\nu_2 + \nu_4$ (CH_4)	combination	5
2591		$2\nu_4$ (CH_4)	overtone	5
	2568	-		
	2229	ν_3 (N_2O)	NN stretch	4
1861		ν_1 ($[NO]_2$)	Symm. NO stretch	4
	1845	ν_1 (N_2O_3)	NO stretch	4
	1793	-		
1758		ν_5 ($[NO]_2$)	Asymm. NO stretch	4
	1608	ν_3 (NO_2)/ ν_2 (N_2O_3)	NO stretch	4
	1560	ν_3 (HNO)	NO stretch	4
1297		ν_4 (CH_4)	Deg. stretch	5

Table S4. Infrared absorption features of $^{13}CH_4$[a] and NO ice mixture before irradiation and new absorption bands observed in the infrared spectrum after irradiation. All measurements have been performed at 5K.

Wavenumber (cm^{-1})		Assignment	Carrier	Ref.
Before irradiation	**After irradiation**			
4520		$\nu_2 + \nu_3$ ($^{13}CH_4$)	combination	
4283		$\nu_3 + \nu_4$ ($^{13}CH_4$)	combination	
4192		$\nu_1 + \nu_4$ ($^{13}CH_4$)	combination	
3594		$\nu_1 + \nu_5$ ($[NO]_2$)	combination	4
2998		ν_3 ($^{13}CH_4$)	CH stretch	
	2977	ν_{10} ($^{13}C_2H_6$)	CH_3 stretch	5
2904		ν_1 ($^{13}CH_4$)	Symm. stretch	
2805		$\nu_2 + \nu_4$ ($^{13}CH_4$)	combination	
2578		$2\nu_4$ ($^{13}CH_4$)	overtone	
	2568	-		
	2229	ν_3 (N_2O)	NN stretch	4
1861		ν_1 ($[NO]_2$)	Symm. NO stretch	4
	1845	ν_1 (N_2O_3)	NO stretch	4
	1793	-		
1758		ν_5 ($[NO]_2$)	Asymm. NO stretch	4
	1608	ν_3 (NO_2)/ ν_2 (N_2O_3)	NO stretch	4
	1560	ν_3 (HNO)	NO stretch	4
1290		ν_4 ($^{13}CH_4$)	Deg. stretch	

[a] O. N. Ulenikov et al., *J. Chem. Phys.* **141**, 234302 (2014).

Table S5. Infrared absorption features of CD_4 and NO ice mixture before irradiation and new absorption bands observed in the infrared spectrum after irradiation. All measurements have been performed at 5K.

Wavenumber (cm^{-1})		Assignment	Carrier	Ref.
Before irradiation	**After irradiation**			
4479		$2\nu_3$ (CD_4)	overtone	[5]
3592		$\nu_1 + \nu_5$ ($[NO]_2$)	combination	[4]
3237		$\nu_3 + \nu_4$ (CD_4)	combination	[5]
3089		$\nu_1 + \nu_4$ (CD_4)	combination	[5]
2250		ν_3 (CD_4)	CH stretch	[5]
	2229	ν_{10} (C_2H_6)	CH_3 stretch	[5]
2090		ν_1 (CD_4)	Symm. stretch	[5]
1861		ν_1 ($[NO]_2$)	Symm. NO stretch	[4]
	1845	ν_1 (N_2O_3)	NO stretch	[4]
	1791			
1758		ν_5 ($[NO]_2$)	Asymm. NO stretch	[4]
	1610	ν_3 (NO_2)/ ν_2 (N_2O_3)	NO stretch	[4]
	1521	ν_3 (HNO)	NO stretch	[4]
989		ν_4 ($^{13}CH_4$)	Deg. stretch	[5]

Table S6. Data applied to calculate the average dose per molecule.

Initial Kinetic energy of the electrons	5 keV
Irradiation current (I)	20 ± 2 nA
Irradiation time (t)	900 s
Average penetration depth, l	317±32 nm
Average kinetic energy of backscattered electrons, E_{bs}[a]	3.8 ± 0.4 keV
Fraction of backscattered electrons, f_{bs}[a]	0.33 ± 0.03
Average kinetic energy of transmitted electrons, E_{trans}[a],	0.0 keV
Fraction of transmitted electrons, f_{trans}[a]	0
Average density of the ice mixture, ρ	0.86 g cm^{-3}
Irradiated area, A	1.0 ± 0.2 cm^2
total number of molecules processed	3.6±0.6 × 10^{17}
dose per molecule, D	Methane: 0.44 ± 0.04 eV
	Nitrogen monoxide: 0.82 ± 0.08 eV
Total number of electrons	1.1±0.1 × 10^{14}

[a] Values from CASINO simulations.

Table S7. Parameters for the vacuum ultraviolet (VUV) light generated in the present study

Photon energy (eV)		**10.49**	**9.95**	**9.92**	**9.50**	**9.00**
$3\omega_1$	Wavelength (nm)	118.19	-	-	-	-
$2\omega_1 - \omega_2$	Wavelength (nm)	-	124.61	124.98	130.51	137.76
ω_1	Wavelength (nm)	355	202.316	202.316	202.316	222.566
Nd:YAG (ω_1)	Wavelength (nm)	355	532	532	532	355
Dye laser (ω_1)	Wavelength (nm)	-	606.948	606.948	606.948	445.132
Dye		-	Rh 610/ Rh 640	Rh 610/ Rh 640	Rh 610/ Rh 640	Coumarin 450
ω_2	Wavelength (nm)	-	537.550	530.648	449.794	579.014
Nd:YAG (ω_2)	Wavelength (nm)	-	355	532	355	532
Dye laser (ω_2)	Wavelength (nm)	-	537.550	-	449.794	579.014
Dye		-	Coumarin 540 A	-	Coumarin 450	Pyrromethane 593
	Nonlinear medium	Xe	Kr	Kr	Kr	Xe

Table S8. Optimized geometrical coordinates of CH_3NO isomers depicted in **Fig. 1**.

Atom	X	Y	Z	Atom	X	Y	Z
		1				**2**	
C	0.690653	-0.322734	0.016325	O	-1.199499	-0.025229	0.000000
H	1.290820	-0.510614	-0.865297	H	0.152698	1.359446	0.000000
H	1.134962	-0.609235	0.963551	H	0.967631	-1.449917	0.000000
O	-0.046241	0.856830	0.021231	H	2.023988	0.128243	0.000000
N	-0.725393	-0.452725	-0.16106	C	1.075279	-0.379035	0.000000
H	-1.122019	-0.629306	0.761369	N	0.000000	0.348325	0.000000
		3				**4**	
C	0.943343	-0.568666	0.000000	C	1.133948	-0.032310	0.000000
H	0.409853	-1.516932	0.000000	H	1.240095	-1.111575	0.000000
H	1.575407	-0.461030	0.880844	H	2.001743	0.609226	0.000000
H	1.575407	-0.461030	-0.880844	N	0.000000	0.539920	0.000000
N	0.000000	0.572263	0.000000	O	-1.028946	-0.403554	0.000000
O	-1.152591	0.230643	0.000000	H	-1.813956	0.145199	0.000000
		5				**6**	
C	0.000000	0.416617	0.000000	C	0.162209	0.385678	0.000823
H	-0.809899	-1.257558	0.000000	O	1.191881	-0.245405	0.004053
H	-0.255725	1.472362	0.000000	H	0.139272	1.485489	0.001121
O	-1.110561	-0.341374	0.000000	N	-1.082769	-0.157485	-0.026935
N	1.156246	-0.089376	0.000000	H	-1.176598	-1.152764	0.056095
H	1.856392	0.642120	0.000000	H	-1.891589	0.418843	0.093967

		7		
H	-1.814281	0.501066	0.000000	
N	-1.147743	-0.269427	0.000000	
O	0.000000	0.418668	0.000000	
C	1.121545	-0.190223	0.000000	
H	1.131757	-1.269569	0.000000	
H	1.987459	0.446483	0.000000	

Table S9. CCSD/cc-pVTZ optimized coordinates of the intermediates, transition states in the reactions of singlet and triplet carbene (CH_2) with nitrosyl hydride (HNO) depicted in **Figure 4.** Coordinates of optimized minimum energy crossing points (MSX) are calculated at the of CPMCSCF/TZVPP level of theory.

Atom	X	Y	Z	Atom	X	Y	Z
Singlet 1				**Singlet 2**			
C	0.690653	-0.322734	0.016325	O	-1.199499	-0.025229	0.000000
H	1.290820	-0.510614	-0.865297	H	0.152698	1.359446	0.000000
H	1.134962	-0.609235	0.963551	H	0.967631	-1.449917	0.000000
O	-0.046241	0.856830	0.021231	H	2.023988	0.128243	0.000000
N	-0.725393	-0.452725	-0.16106	C	1.075279	-0.379035	0.000000
H	-1.122019	-0.629306	0.761369	N	0.000000	0.348325	0.000000
Singlet 7				**Singlet TS 2-1**			
H	-1.814281	0.501066	0.000000	C	0.941223	0.272978	0.016152
N	-1.147743	-0.269427	0.000000	H	0.931283	1.145356	-0.616148
O	0.000000	0.418668	0.000000	H	1.732316	0.141859	0.751264
C	1.121545	-0.190223	0.000000	O	-1.035323	0.350485	0.096852
H	1.131757	-1.269569	0.000000	N	0.001418	-0.613064	-0.198615
H	1.987459	0.446483	0.000000	H	-0.038271	-1.437513	0.38346
Singlet TS 1-7				**Singlet TS 2-7**			
C	0.992584	-0.248209	0.022614	C	-1.944011	-0.087036	-0.184716
H	1.852339	-0.007043	-0.591663	H	-1.877128	-0.79235	0.666689
H	0.919938	-1.159885	0.589915	H	-1.924745	0.893239	0.330227
O	0.018157	0.619288	0.078436	O	0.86918	0.644756	0.008033
N	-1.032226	-0.305979	-0.196725	N	0.953396	-0.55556	0.066153
H	-1.647453	-0.156268	0.615646	H	1.83873	-0.847801	-0.415952

Triplet 1				Triplet 2			
C	0.000000	0.550630	0.000000	O	1.123151	-0.336145	0.089199
H	-0.080841	1.180007	0.894827	H	0.249411	1.409886	0.083639
H	-0.080841	1.180007	-0.894827	H	-1.403298	-0.957210	-0.650713
O	1.118556	-0.241191	0.000000	H	-1.670712	-0.018909	0.952594
N	-1.144604	-0.347013	0.000000	C	-1.168444	-0.131790	0.001356
H	-0.774537	-1.305182	0.000000	N	0.121437	0.435163	-0.158179
Triplet 3				**Triplet TS 2**			
C	-1.129983	-0.208859	-0.070376	N	0.54937	0.491637	-0.038203
H	-2.013216	0.406606	-0.041485	O	1.355879	-0.403841	-0.066668
H	-1.092820	-1.225091	0.287867	C	-1.796368	-0.132303	-0.027659
O	0.038270	0.525083	0.050410	H	-2.086221	-0.893815	0.6798
N	1.099302	-0.348425	-0.030393	H	-2.374838	0.550467	-0.62753
H	1.884657	0.309947	-0.014662	H	0.546643	0.926437	0.914453
Triplet TS 1-7				**Triplet TS 2-i1**			
C	-0.829815	-0.347126	0.000052	C	-1.140114	-0.266674	0.03894
H	-1.302281	-0.619986	0.934265	H	-1.28033	-1.139565	-0.582779
H	-1.302282	-0.620174	-0.934086	H	-1.793508	-0.111681	0.890239
O	-0.066166	0.830951	-0.00006	O	1.363879	-0.267278	0.084441
N	0.920326	-0.504721	-0.000089	N	-0.134438	0.52561	-0.231637
H	1.670491	0.208357	0.000618	H	-0.055443	1.310237	0.404829
Triplet TS i1-1				**1-MSX**			
C	-0.332084	-0.620015	0.040168	C	-0.024572	0.508920	-0.040766
H	-0.166115	-1.284207	-0.799531	H	-0.071569	1.063889	0.896150
H	-0.105238	-1.028864	1.023395	H	-0.053475	1.233106	-0.847539
O	1.378601	0.258199	-0.017554	O	1.193647	-0.140577	-0.047069
N	-1.078430	0.436032	-0.151653	N	-1.147582	-0.373046	-0.150586
H	-1.215937	0.915349	0.737136	H	-0.858716	-1.275034	0.189811

2-MSX				3-MSX			
O	1.110648	-0.311636	0.152641	H	1.850867	-0.376486	-0.141154
H	0.249766	1.391375	0.041402	N	1.114024	0.308982	-0.089094
H	-1.434938	-0.917341	-0.665502	O	0.049219	-0.433791	0.306323
H	-1.626379	-0.071731	0.967704	C	-1.085781	0.241105	-0.054485
C	-1.172337	-0.115331	-0.006075	H	-1.222956	1.207472	0.393486
N	0.124786	0.425658	-0.172273	H	-1.919381	-0.406530	-0.232793
Triplet TS 2-7				**Triplet i1**			
C	1.069094	0.03804	0.010099	C	1.187614	-0.537585	-0.000099
H	1.435518	-0.291843	-0.947453	H	0.482987	-1.364101	0.009967
H	1.439329	-0.364631	0.939028	H	2.247933	-0.791988	-0.012220
N	-0.520047	-0.605635	-0.028038	O	-2.062401	-0.058413	-0.001210
O	-0.526022	0.713307	0.006735	N	0.734463	0.647367	0.002873
H	-1.440903	-1.038772	0.090217	H	1.501367	1.317336	-0.007580
Triplet TS 7							
N	-1.209474	0.37319	0.058056				
O	-0.374774	-0.537815	0.07836				
C	1.576741	0.135957	0.02942				
H	1.579212	1.214462	0.057041				
H	2.221176	-0.564484	-0.477311				
H	-1.796331	0.224466	-0.789524				

Table S10. Singlet adiabatic CCSD/cc-pVTZ//CCSD(T)/CBS ionization energies (IE) and relative energies of the CH_3NO isomers depicted in Fig. 1.

	CCSD/ cc-pVTZ + E_{zpc} [a]	E_{zpc} [b]	CCSD(T)/cc-pVDZ	CCSD(T)/cc-pVTZ	CCSD(T)/cc-pVQZ	CCSD(T)/ CBS	IE(eV)[c]	E(kJ/mol)[d]
1	-169.457841	0.046522	-169.355047	-169.531763	-169.584062	-169.613293	0.00	297
1^+	-169.105519	0.045654	-169.012158	-169.177308	-169.225453	-169.252277	9.80	
2	-169.465423	0.045943	-169.365013	-169.542005	-169.596174	-169.626662	0.00	260
2^+	-169.135853	0.045350	-169.042546	-169.203875	-169.252101	-169.279113	9.44	
3	-169.471792	0.043853	-169.373485	-169.543152	-169.594915	-169.624029	0.00	262
3^+	-169.139424	0.043900	-169.051373	-169.209784	-169.257399	-169.284099	9.25	
4	-169.490210	0.045177	-169.387952	-169.562654	-169.615268	-169.644784	0.00	211
4^+	-169.129535	0.044504	-169.036696	-169.199405	-169.247913	-169.275069	10.04	
5	-169.552342	0.046918	-169.4475689	-169.6252707	-169.6788789	-169.7089626	0.00	47
5^+	-169.186126	0.043946	-169.0898385	-169.2530731	-169.3018311	-169.3291368	10.25	
6	-169.569833	0.045997	-169.464166	-169.641590	-169.695524	-169.725838	0.00	0
6^+	-169.206128	0.046256	-169.112814	-169.274554	-169.322597	-169.349471	10.25	
7	-169.401056	0.043983	-169.305940	-169.480739	-169.533027	-169.562318	0.00	424
7^+	-169.106803	0.043557	-169.014083	-169.173869	-169.220886	-169.247134	8.57	

[a] CCSD/cc-pVTZ energy with zero-point energy correction in hartree.

[b] zero-point energy by CCSD/cc-pVTZ in hartree.

[c] Ionization energy by CCSD(T)/CBS with CCSD/cc-pVTZ zero-point energy correction.

[d] relative energy by CCSD(T)/CBS with CCSD/cc-pVTZ zero-point energy correction.

Table S11. CCSD/cc-pVTZ//CCSD(T)/CBS energies on the adiabatic singlet (^{1}) and triplet (^{3}) ground state potential energy surfaces, of all the reactants, intermediates, and transition states depicted in **Figure 4** along with CPMCSCF/TZVPP//CCSD(T)/CBS energies of minimum-energy crossing points (MSX).

	CCSD/ cc-pVTZ + E_{zpc} [a]	E_{zpc} [b]	CCSD(T)/ cc-pVDZ	CCSD(T)/ cc-pVTZ	CCSD(T)/ cc-pVQZ	CCSD(T)/ CBS	E[c] (kJ/mol)
$^1CH_2$	-39.039820	0.016745	-39.022144	-39.061382	-39.071910	-39.077667	
$^3CH_2$	-39.057040	0.017425	-39.041349	-39.077852	-39.087330	-39.092472	
^{1}HNO	-130.264419	0.014238	-130.170806	-130.298284	-130.338058	-130.360531	
H	-0.502156	0.000000	-0.499278	-0.499810	-0.499946	-0.500019	
$^1CH_2$+^{1}HNO	-169.304239	0.030983	-169.192950	-169.359666	-169.409969	-169.438198	37
$^3CH_2$+^{1}HNO	-169.321459	0.031663	-169.212155	-169.376136	-169.425388	-169.453003	0.0
^{1}1	-169.457841	0.046522	-169.355047	-169.531763	-169.584062	-169.613293	-382
^{1}2	-169.465423	0.045943	-169.365013	-169.542005	-169.596174	-169.626662	-418
^{1}7	-169.401056	0.043983	-169.305940	-169.480739	-169.533027	-169.562318	-255
^{1}TS 2-1	-169.377174	0.043230	-169.274594	-169.453049	-169.507184	-169.537598	-192
^{1}TS 1-7	-169.372617	0.042119	-169.279482	-169.453696	-169.505173	-169.533936	-185
^{1}TS 2-7	-169.305546	0.033430	-169.197772	-169.363891	-169.413986	-169.442096	33
^{3}1	-169.414829	0.041447	-169.306381	-169.477205	-169.528358	-169.557020	-247
^{3}2	-169.400855	0.042008	-169.292416	-169.465376	-169.517810	-169.547265	-220
^{3}7	-169.384607	0.041088	-169.277066	-169.448340	-169.499098	-169.527476	-171
^{3} TS 2	-169.316276	0.034078	-169.209378	-169.373893	-169.423722	-169.451708	10
^{3} TS 7	-169.302691	0.034598	-169.196919	-169.362039	-169.412062	-169.440158	41
^{3} TS 1-7	-169.289627	0.038808	-169.183692	-169.358036	-169.409199	-169.437744	59
^{3}TS 2-7	-169.292393	0.038475	-169.184880	-169.359465	-169.410971	-169.439741	53
^{3}TS 1-i1	-169.372198	0.041043	-169.2685432	-169.4353343	-169.4854098	-169.5134831	-134
^{3}TS 2-i1	-169.364696	0.041041	-169.2612389	-169.4297177	-169.4803793	-169.5087904	-122
1-MSX		0.044606	-169.306981	-169.478098	-169.529116	-169.557677	-241
2-MSX		0.044346	-169.290405	-169.464167	-169.516773	-169.546316	-212
7-MSX		0.043522	-169.272661	-169.444914	-169.495946	-169.524476	-157

[a] CCSD/cc-pVTZ energy with zero-point energy correction in hartree.
[b] zero-point energy by CCSD/cc-pVTZ in hartree.
[c] relative energy by CCSD(T)/CBS with CCSD/cc-pVTZ zero-point energy correction.

Table S12. CCSD/cc-pVTZ optimized coordinates of the structures depicted in **Fig. S15.**

1				$1^{/}$			
C	0.690653	-0.322734	0.016325	C	-0.690665	-0.322713	0.016328
H	1.290820	-0.510614	-0.865297	H	-1.135020	-0.609190	0.963542
H	1.134962	-0.609235	0.963551	H	-1.290803	-0.510599	-0.865319
O	-0.046241	0.856830	0.021231	O	0.046272	0.856831	0.021228
N	-0.725393	-0.452725	-0.16106	N	0.725375	-0.452748	-0.161055
H	-1.122019	-0.629306	0.761369	H	1.122009	-0.629352	0.761371
TS $1\text{-}1^{/}$							
C	0.693183	0.355193	-0.000006				
H	1.236611	0.563536	0.918181				
H	1.236107	0.563492	-0.918528				
O	-0.04001	-0.874756	-0.000007				
N	-0.668887	0.437732	0.000104				
H	-1.629529	0.675737	-0.000294				

Table S13. CCSD/cc-pVTZ//CCSD(T)/CBS energies on the adiabatic singlet ground state potential energy surface of the structures depicted in **Fig. S15.**

	CCSD/ cc-pVTZ + E_{zpc} [a]	E_{zpc} [b]	CCSD(T)/ cc-pVDZ	CCSD(T)/ cc-pVTZ	CCSD(T)/ cc-pVQZ	CCSD(T)/ CBS	E^c (kJ/mol)
^{1}c1 (C_1, ^{1}A)	-169.457841	0.046522	-169.355047	-169.531763	-169.584062	-169.613293	0.0
^{1}c1' (C_1, ^{1}A)	-169.457841	0.046522	-169.355048	-169.531763	-169.584062	-169.613294	0.0
^{1}tsc1c1' (C_1, ^{1}A)	-169.401857	0.044121	-169.2918105	-169.4725078	-169.5263645	-169.5565119	143

[a] CCSD/cc-pVTZ energy with zero-point energy correction in hartree.
[b] zero-point energy by CCSD/cc-pVTZ in hartree.
[c] relative energy by CCSD(T)/CBS with CCSD/cc-pVTZ zero-point energy correction.

References:

1. B. M. Jones and R. I. Kaiser, *J. Phys. Chem. Lett.*, 2013, **4**, 1965-1971.
2. S. Maity, R. I. Kaiser and B. M. Jones, *Phys. Chem. Chem. Phys.*, 2015, **17**, 3081-3114.
3. C. J. Bennett, S. H. Chen, B. J. Sun, A. H. H. Chang and R. I. Kaiser, *Astrophys. J.*, 2007, **660**, 1588-1608.
4. S. Góbi, P. B. Crandall, P. Maksyutenko, M. Förstel and R. I. Kaiser, *J. Phys. Chem. A*, 2018, **122**, 2329-2343.
5. R. I. Kaiser, S. Maity and B. M. Jones, *Phys. Chem. Chem. Phys.*, 2014, **16**, 3399-3424.
6. D. Drouin, A. R. Couture, D. Joly, X. Tastet, V. Aimez and R. Gauvin, *Scanning*, 2007, **29**, 92-101.
7. K. A. Peterson and T. H. Dunning, *J. Phys. Chem.*, 1995, **99**, 3898-3901.
8. P. J. K. H.-J. Werner, G. Knizia, F. R. Manby, M. Schütz, P. Celani, W. Györffy, D. Kats, T. Korona, R. Lindh, A. Mitrushenkov, G. Rauhut, K. R. Shamasundar, T. B. Adler, R. D. Amos, S. J. Bennie, A. Bernhardsson, A. Berning, D. L. Cooper, M. J. O. Deegan, A. J. Dobbyn, F. Eckert, E. Goll, C. Hampel, A. Hesselmann, G. Hetzer, T. Hrenar, G. Jansen, C. Köppl, S. J. R. Lee, Y. Liu, A. W. Lloyd, Q. Ma, R. A. Mata, A. J. May, S. J. McNicholas, W. Meyer, T. F. Miller III, M. E. Mura, A. Nicklass, D. P. O'Neill, P. Palmieri, D. Peng, K. Pflüger, R. Pitzer, M. Reiher, T. Shiozaki, H. Stoll, A. J. Stone, R. Tarroni, T. Thorsteinsson, M. Wang, and M. Welborn, *{WIREs Comput Mol Sci}*, 2012, **{2}**, {242--253}.
9. M. J. T. Frisch, G. W.; Schlegel, H. B.; Scuseria, G. E.; Robb, M. A.; Cheeseman, J. R.; Scalmani, G.; Barone, V.; Petersson, G. A.; Nakatsuji, H.; Li, X.; Caricato, M.; Marenich, A. V.; Bloino, J.; Janesko, B. G.; Gomperts, R.; Mennucci, B.; Hratchian, H. P.; Ortiz, J. V.; Izmaylov, A. F.; Sonnenberg, J. L.; Williams-Young, D.; Ding, F.; Lipparini, F.; Egidi, F.; Goings, J.; Peng, B.; Petrone, A.; Henderson, T.; Ranasinghe, D.; Zakrzewski, V. G.; Gao, J.; Rega, N.; Zheng, G.; Liang, W.; Hada, M.; Ehara, M.; Toyota, K.; Fukuda, R.; Hasegawa, J.; Ishida, M.; Nakajima, T.; Honda, Y.; Kitao, O.; Nakai, H.; Vreven, T.; Throssell, K.; Montgomery, J. A., Jr.; Peralta, J. E.; Ogliaro, F.; Bearpark, M. J.; Heyd, J. J.; Brothers, E. N.; Kudin, K. N.; Staroverov, V. N.; Keith, T. A.; Kobayashi, R.; Normand, J.; Raghavachari, K.; Rendell, A. P.; Burant, J. C.; Iyengar, S. S.; Tomasi, J.; Cossi, M.; Millam, J. M.; Klene, M.; Adamo, C.; Cammi, R.; Ochterski, J. W.; Martin, R. L.; Morokuma, K.; Farkas, O.; Foresman, J. B.; Fox, D. J., *Gaussian 16, Revision C.01, Gaussian, Inc., Wallingford CT, 2016*.
10. C. J. Bennett, S. J. Brotton, B. M. Jones, A. K. Misra, S. K. Sharma and R. I. Kaiser, *Anal. Chem.*, 2013, **85**, 5659-5665.